53rd 3AF International Conference on Applied Aerodynamics
26 – 28 March 2018, Salon de Provence – France

FP51-2018-simiriotis

Best article award of the 53th AERO2018 attributed by the French Association 3AF Salon-de-Provence, March 2018 -cf. last page

Electroactive morphing on a supercritical wing targeting improved aerodynamic performance and flow control in high Reynolds numbers

N. Simiriotis[(1)], G. Jodin[(2)], A. Marouf[(3)], Y. Hoarau[(4)], J.F. Rouchon[(5)] and M. Braza[(6)]

[(1)]*IMFT UMR 5502, 2 Alle du Professeur Camille Soula, 31400 Toulouse, France, nikolaos.simiriotis@imft.fr*

[(2)]*LAPLACE UMR 5213/IMFT UMR 5502, 2 rue Charles Camichel, 31071 Toulouse, France, jodin@laplace.univ-tlse.fr*

[(3)]*ICUBE UMR7357/IMFT UMR 5502, 300 Bd Sébastien Brant, 67400 Strasbourg, France, abderahmane.marouf@etu.unistra.fr*

[(4)]*ICUBE, UMR7357, 300 Bd Sébastien Brant, 67400 Strasbourg, France, hoarau@unistra.fr*

[(5)]*LAPLACE, UMR 5213, 2 rue Charles Camichel, 31071 Toulouse, France, rouchon@laplace.univ-tlse.fr*

[(6)]*IMFT, UMR 5502, 2 Alle du Professeur Camille Soula, 31400 Toulouse, France, marianna.braza@imft.fr*

ABSTRACT

This article examines the morphing effects of the trailing-edge deformation and vibration on the turbulent structures in the wake of a supercritical Airbus-320 wing. The Reynolds number was 1 Million. The study is carried out in the low subsonic regime at an incidence angle of 10^o, corresponding to take-off/landing flight phases. The morphing effects on the aerodynamic coefficients are discussed in order to identify optimal frequency/amplitude ranges for the vibrations imposed by composite piezo-actuators, disposed along the span of the wing. Time-Resolved PIV measurements taken from the subsonic wind tunnel are investigated together with numerical simulations. Morphing effects on the coherent structures in the wake have been analysed by means of Proper Orthogonal Decomposition. It has been shown that specific frequency/amplitude ranges are able to produce an enhanced aerodynamic performance and suppress instability modes associated with noise sources.

1. INTRODUCTION

This study aims at completing previous studies carried out at the Institut de Mécanique des Fluides de Toulouse - IMFT that highlight the capacity of morphing to increase lift, decrease drag and reduce the amplitude of instability modes associated to aerodynamic noise. Morphing from hereby after will be referring to the adaptation of the real-time shape and vibrational behaviour of the aerodynamic surface. In this context, a multi-disciplinary research platform involving the LAPLACE (Laboratoire Plasma et Conversion d'Energie) and IMFT French Laboratories has been continuously working in this topic since 2010, originally thanks to the support of the Foundation STAE (*h*ttp://www.fondation-stae.net/). By this synergistic platform among six Institutes in Toulouse (*www.smartwing.org*) coordinated by IMFT and in close collaboration with AIRBUS *Emerging Technologies and Concepts Toulouse*, advanced *electroactive* morphing designs for the wings of the future are currently being developed and studied (*https://lejournal.cnrs.fr/videos/les-ailes-du-futur*). In particular, the *hybrid* morphing concept, partly bio-inspired, was developed ([11], [8]) to operate at different time scales. This concept enables the manipulation of the near-region turbulence enhancing specific beneficial structures in the wake. In this way and thanks to the introduction of smaller-scale chaotic turbulent vortices, breaking down or suppression of pre-existing predominant instability modes can be achieved. Activating a shear sheltering effect leading to a considerable thinning of the separated shear layers, it has been rendered possible to increase the aerodynamic performance and simultaneously decrease the noise sources.

This study focuses in high Reynolds number (order of 10^6). Previous studies in the literature were carried out at low Reynolds numbers [7], [15] examined part of the flow characteristics and although useful in the analysis, are quite limited and not operating in multiple scales. Past papers have also examined the forcing of the trailing of a wing [4] also in lower Reynolds number. The flow in the supercritical Reynolds range presents complex vortex

dynamics and interactions with the solid structure, calling for specific attention in order to produce successful morphing effects. High Reynolds dynamics change the general flow behaviour and the morphing practices and targets. In the present context, the electro-active morphing is a more general strategy than standard flow control techniques as it creates fluid-structure interactions and inter-optimality among structural dynamics and turbulence manipulation.

In the present article, the electroactive morphing effects around an A320 wing are presented at a Reynolds number of 1 million and an angle of incidence of 10^o, by means of numerical simulation and experimental investigation.This study is in the context of the H2020 EU SMS

2. EXPERIMENTAL PROCEDURE

The present article follows the experimental work of G. Jodin [8] on a reduced scale hybrid morphing prototype embedding both camber control and Higher Frequency Vibrating Trailing Edge (HFVTE) actuators. Measurements for a Reynolds number of 1 million are considered to provide an inter-validation between the experimental and the numerical studies following. In this analysis, the electroactive morphing effects of the higher frequency vibration and slight deformation of the Multi-Fiber composite piezo-actuators in the trailing edge region (Fig. 1) will be studied. The piezoelectric patches were glued on both sides of a metallic substrate and are alternatively activated to reach deformations with amplitudes up to $0.5mm$. In order to maintain the trailing edge shape, the assembly is covered by silicone, specifically designed to limit the impact on the actuator's performance. The technical characteristics for the electro-active hybrid morphing actuation are extensively described in [9]

At a given controlled camber, the vibrating trailing edge creates small-scale turbulent eddies and adds kinetic energy in the wake that provokes interactions in the upper and lower shear layer. This aims at enhancing the super-critical character of the flow and producing an eddy-blocking effect constricting the shear layers as mentioned in [8]. By enriching this region with chaotic vortices, the target is to attenuate specific coherent structure generation associated with the wake's width (form drag), feedback effects on the lift and noise sources. This eddy-blocking concept was first studied numerically in [14] for a transonic flow around a supercritical airfoil and put in evidence experimentally thanks to the electro-active morphing [12].

The time Resolved Particle Image Velocimetry (TR-PIV) measurements will be re-examined in this paper. The most probable displacement of the particles between consecutive images is obtained from the cross-correlation plane of consecutive images. The sampling rate was about $10KHz$. Particle images are recorded during the experiment using a digital high-speed camera focused in the mid-section concerning the depth of the field (the laser sheet representation can be found placed in the streamwise direction as depicted in Fig. 1). The thickness of the laser sheet was 2.5 mm. For the experimental procedure smoke particles of $3.4\mu m$ diameter were introduced in the airflow giving a Stokes number $Sk = 5 \cdot 10^{-4}$ which allows the particles follow consistently the motion of the fluid.

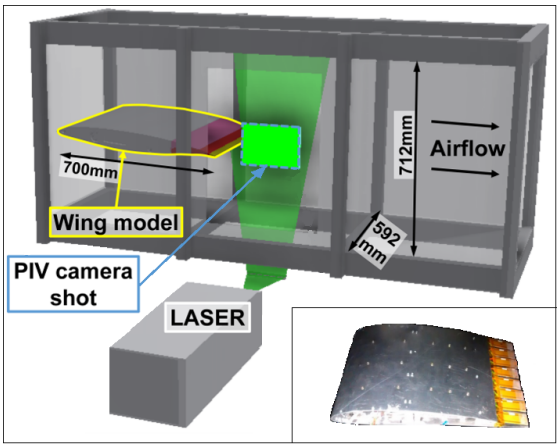

Figure 1: Schematic representation of the experimental test section of the S4 wind tunnel of IMFT with the Airbus-320 wing mounted [8] and illustration of the trailing-edge piezo-actuators along the prototype's span [13].

The wing with a chord dimension of $0.7m$ was placed at an incident angle of 10^o. The incoming velocity was held constant at $(21.5m/s)$, which for reference values of temperature $(293K)$ and pressure $(101325Pa)$ corresponds to a (chord) Reynolds number of 1 million. The velocity variation was evaluated over multiple experiments was estimated to be below 1.5% while the blockage ratio was found to be acceptable as long as the focus is the relative effects of the morphing application. The turbulence intensity of the inlet section of the wind tunnel was estimated at about 0.1% of the free stream velocity. The experimental benchmark was also equipped with an aerodynamic balance in order to measure the lift and drag forces. A more detailed description of the experimental equipment and procedure can be found to [8].

3. NUMERICAL APPROACH & TURBULENCE MODELLING

The complete time dependent compressible Navier-Stokes equations have been solved under the conservative form using the Navier-Stokes Multi-Block (NSMB) code [6], in both two and three dimensions. The computational domain is subdivided into a number of quadrilateral (2D) and hexahedral (3D) grid cells resulting in a

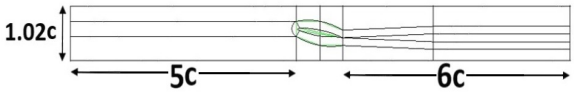

(a) Multi block description of the computational domain.

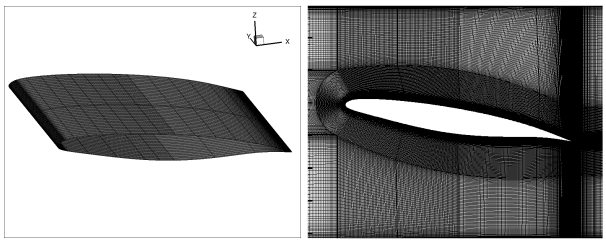

(b) 3D surface meshing of the A320 wing.

(c) 2D mesh around the A320 wing.

Figure 2: Computational domain and mesh.

structured mesh. The multi-block strategy is followed in accordance to the parallelization procedure of the code. A separate discretization of the equations in space and time is applied.

Finite volume cells of constant size in time are considered for the discretization in space. A fourth order standard central skew-symmetric spatial scheme with artificial second and fourth order dissipation terms was used for the convection terms and a second-order central scheme for the diffusion terms. For the temporal discretization, dual time-stepping with a second order implicit backward difference scheme is performed [5]. The artificial compressibility method was implemented in the preconditioning of the flow to increase accuracy in the low subsonic regime.

Both 3D and 2D meshes (Fig. 2) were developed. For the standard 2D mesh, about 300000 finite volume cells were added to the computational domain. The respective 3D mesh was a simple extrusion of the initial 2D mesh in the third dimension, constructed by adding points in the span-wise direction leading to a total mesh size close to 10 million. A refined version of the 2D mesh was also tested. Theses grid sizes were selected after thorough numerical studies. The physical time-step was kept constant in all the computations at 10^{-5} giving a CFL number around 50. About $60-80$ inner iterations were carried out for each time-step.

The upper and lower walls of the tunnel were considered by means of non-slip and slip boundary conditions. After numerical tests that indicated no considerable effect due to the respective boundary layers on the wake development, they have been given a no-slip condition. The inlet velocity was held constant at $21.5m/s$ with a turbulence intensity of 1% to establish matching levels of turbulence with the experimental setup.

In the present work the Organized Eddy Simulation (OES) approach [2], [14] has been employed. Based on the ensemble (phase) averaging of the flow, this approach is sensitized to allow coherent structures and their related instabilities to develop in the high Reynolds number range and is well adapted for detached flows, both typical of all aeronautical applications. The OES approach is non-inherently 3D and therefore can be applied in 2D simulations with sufficient accuracy in capturing the main coherent structure dynamics and their modification. Therefore, it provides a robust method for capturing physical phenomena and treating near wall turbulence. A more detailed description of the OES can be found in [2] and [14].

4. EXPERIMENTAL STUDY - TRPIV

Fig. 3 presents the instantaneous velocity field measured by means of TRPIV, with the contribution of the Signal and Image processing service of IMFT (S. Cazin and M. Marchal). The post-processing of the raw PIV results was carried out with the CPIV-IMFT software, developed with the contribution of the software services of IMFT (P. Elyakime) for parallel (MPI) post-treatment of the results in supercomputing architectures. The plane section depicted in this figure corresponds to the laser sheet placed in the mid-span region.

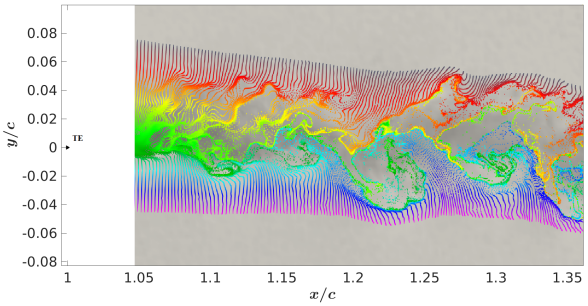

Figure 3: Instantaneous stream velocity from the TRPIV measurements, visualizations by streaklines for $Re = 1M$, angle of attack $a_o = 10^o$.

Temporal signals of the vertical velocity component have been extracted in selected positions downstream of the trailing edge and the corresponding Fast Fourier Transform (FFT) on these signals provide the turbulence spectra. Plots of the Power Spectral Density are presented in Fig. 4b and Fig. 4c for two points selected in the near wake region (see Fig. 4a).

The predominant frequency bump shown in these spectra corresponds to the shear layer's vortex emission, a coherent pattern smeared by chaotic turbulence motion. The characteristic frequency of the shear layer instability is found to be at $254Hz$ as indicated by the signal acquired from monitor point 2. This primary instability is a result of the interactions between the lower and upper shear layers. The vortex shedding developed further

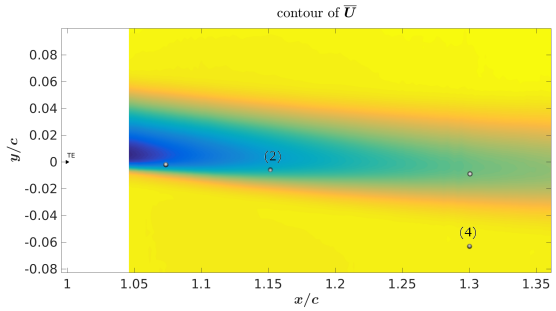

(a) Position of the selected monitor points along the wake; the trailing edge is noted with a symbol.

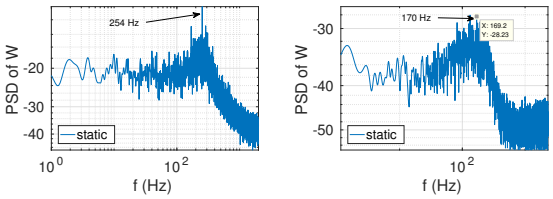

(b) Spectrum from monitor point 2.

(c) Spectrum from monitor point 4.

Figure 4: Spectral content of the vertical velocity component in the near wake region from TRPIV results.

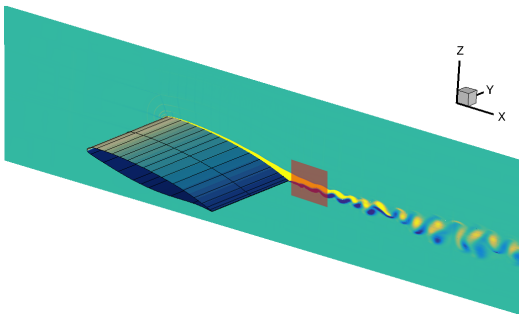

(a) Surface pressure and y vorticity component on a plane section; the rectangular represents the plane of the PIV measurements for which all the comparisons will take place.

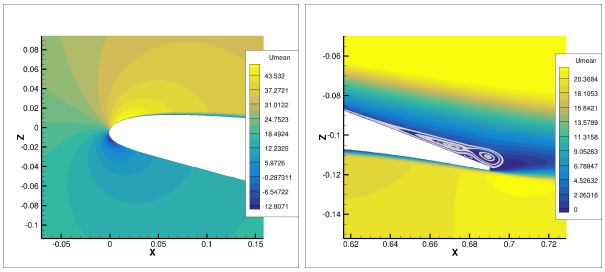

(b) Averaged stream velocity close to the leading edge.

(c) Averaged stream velocity close to the trailing edge.

Figure 5: Global view of the predicted flow field by means of numerical simulation for $Re = 1M$, angle of attack $a_o = 10^o$.

downstream takes place at frequencies around $170Hz$. The monitor point 4 is placed just below the wake in order to give a clear indication of the vortex shedding pattern which is analysed in more detail by means of the numerical simulation because as it is more pronounced in the downstream areas not captured by the PIV plane.

The frequency of the von Kármán shedding corresponds to a Strouhal number close to 0.34 for a characteristic length equal to the initial wake's width. This value is in agreement with the respective ones measured for circular cylinder in supercritical flow conditions [10]. The bumpy image of the spectra indicates non-linear effects between the coherent vortex shedding and the finer scale chaotic turbulent motion. A detailed study of the PIV measurements by a Proper Orthogonal Decomposition (POD) is included in [8] and allows distinguishing the coherent from the chaotic effects.

5. NUMERICAL STUDY

The numerical simulations have been carried out respecting the afore mentioned experimental conditions. A mesh was constructed depicting faithfully the geometry of test section. In this section, the stream-wise direction for the computations is the orientation of the x axis and the vertical direction is that of the z axis, leaving y axis along the span-wise direction. For the validation of the static case, the 3D and the two version of the 2D mesh were used while for the morphing tests, only the standard 2D mesh is considered as it is proven more efficient in terms of computational cost for an extensive multi-parametric study.

Fig. 5 provides a global view over the computational domain and the solution acquired by means of numerical simulation. The flow coming from the inlet moves downstream (from left to right from hereby after). A small detachment at the trailing edge of the wing is evident (Fig. 5c) resulting to the unstable wake region following right after.

The comparison for the time averaged velocity profiles is depicted in Fig. 6a. The agreement between the measured and computed profiles is quite good, even for the 2D case presented in this figure. In Fig. 6b and 6c a comparison between the various numerical tests and the experiments is presented. The calculation for the displacement and momentum thickness in the wake follows eq. 1 and 2, where $u_{99\%} = 0.99 \cdot U_{inlet}$ and $z^*_{99\%}$ the vertical positions along the wake where this is achieved.

$$\delta^* = \int_{z^{low}_{99\%}}^{z^{up}_{99\%}} (1 - \frac{u}{u_{99\%}}) dz \tag{1}$$

$$\theta = \int_{z^{low}_{99\%}}^{z^{up}_{99\%}} \frac{u}{u_{99\%}} (1 - \frac{u}{u_{99\%}}) dz \tag{2}$$

The agreement between the experimental data and the

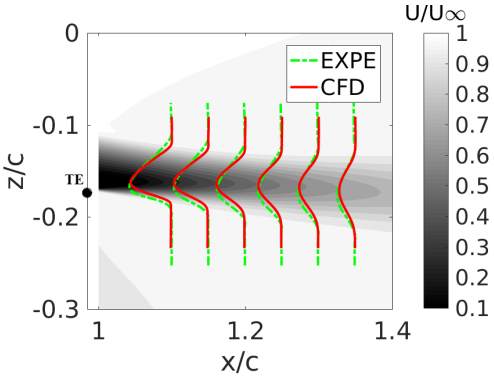

(a) Averaged axial velocity profiles; comparison between the standard 2D simulation and the experimental results; trailing edge noted with a symbol.

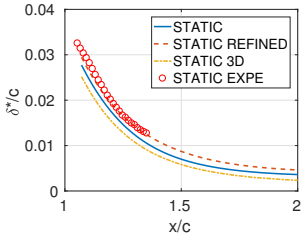

(b) Dispalcement thickness.

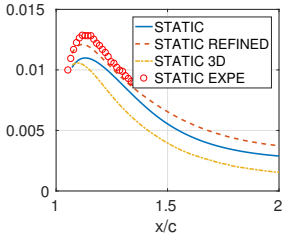

(c) Momentum thickness.

Figure 6: Quantitative comparison of the computational test with the TR-PIV results (STATIC EXPE); numerical tests for: standard 2D mesh (STATIC), a refined 2D mesh (STATIC-REFINED), a 3D mesh (STATIC 3D).

computational results is quite satisfactory. Fig. 7 attests to this as well. It is evident that the main dynamics involved in the wake development can be accurately captured even by the standard 2D mesh. The width of the spectral bump is well captured both close to the trailing edge (primary instability) and further downstream in the wake where the shedding is fully developed (secondary instability). The vortex structure dynamics and their nonlinear interactions can be visualized using streaklines in the wake, pictured in Fig.7a. The unstable shear layer develops global predominant frequencies (around $220Hz$) close to the trailing edge. The lower and upper shear layers interact with each other yielding a von Kármán vortex street further downstream. The vortex shedding is placed around $165Hz - 185Hz$, which compares well with the value obtained from the experiments. These effects are also highlighted by the POD performed on the computational results.

5.1 Electroactive Morphing on the Trailing Edge

The motion and slight deformation of the near-trailing edge region due to the $4mm$ long MFC piezo-actuators vibrating with an amplitude of order $0.5mm$. The Arbi-

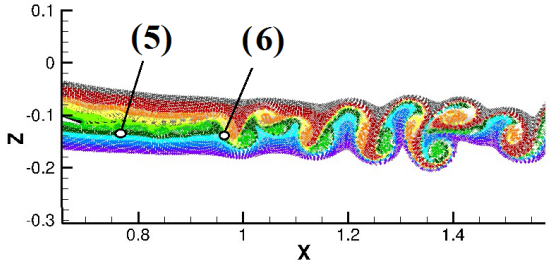

(a) Position of the monitor points in the computational domain along the wake.

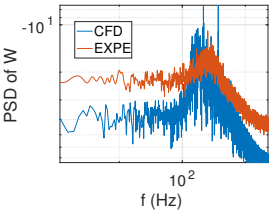

(b) Spectrum from monitor point 5.

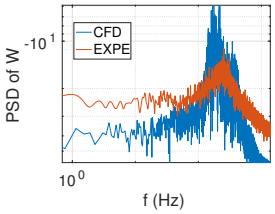

(c) Spectrum from monitor point 6.

Figure 7: Streaklines (top) and spectral content (bottom) of the near wake region, comparison between computational (standard 2D mesh) and experimental results.

trary Lagrangian-Eulerian methodology [3] is applied for the calculation of the variables in the deformable/moving grid. The applied deformation in the trailing edge region follows closely the polynomial deformation applied on the reduced scale prototype. The frequency of the vibration f_a and the amplitude A_o of the sinusoidal time variation are left to be imposed in each test case. The amplitude corresponds to the maximum displacement, i.e. the displacement of the ending tip of the trailing edge. In the tests following, the effect of the aerodynamic forces on the vibrational behaviour of the piezoactuators has not been taken into account (one-way fluid-structure interaction) since they have been evaluated as negligible in [9].

- EFFECTS ON THE WAKE DYNAMICS

The morphing seems to have prominent effects on the development of vortical structures in the wake as exhibited in Fig. 8 where visualizations by streaklines are presented, in comparison with Fig. 7a where no morphing was applied. The amplitude of the vibration was held constant at $0.35mm$ while the actuation frequency was left to vary. In the experiments this amplitude value was the largest one tested with the specific morphing implementation. For frequencies lower than the one related to the shear layer instability, the flow seems unaffected by the perturbation travelling at a much lower propagation speed. For an actuation close to the instability frequency ($f_a = 200Hz$), some kind of resonance phenomena seem to take place. A "lock-in" to the morphing frequency is

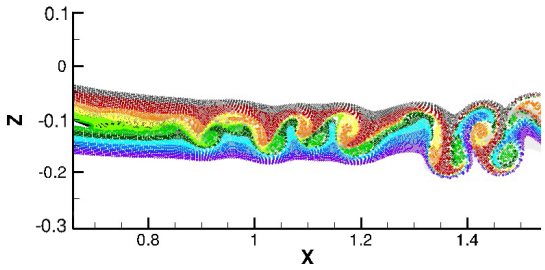

(a) $f_a = 60Hz$

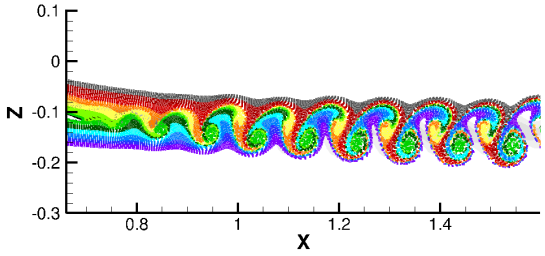

(b) $f_a = 200Hz$

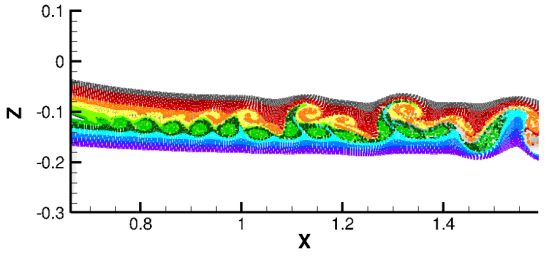

(c) $f_a = 300Hz$

Figure 8: Development of vortical structures in the wake, visualization with streaklines, calculation my means of numerical simulation. The amplitude is set at $0.35mm$ for every actuating frequency.

achieved, non-linear interactions seem to be suppressed and large coherent highly energetic structures are developed resembling clearly a vortex sheet. When the morphing frequency further increases ($f_a = 300Hz$), the flow seems able to follow the much faster perturbation. The "lock-in" mechanism remains (only to become weaker for even higher frequencies) and smaller vortices get generated resulting to a much thinner wake region. The shear layer seems to be enforced and a convective instability leads to the suppression of the shedding mechanism up to further downstream.

- MEAN EFFECTS ON THE WAKE

In this section a comparison on the time averaged results is carried out. In Fig. 9 the mean axial velocity profiles are plotted along the wake for various x/c positions, where the x axis is zero at the leading edge of the wing. It is evident that for frequencies lower than the natural ones of the flow (i.e. for $60Hz$ and $100Hz$) only slight changes in the profiles are visible and mostly at the early x/c stations, close to the trailing edge. For an actuation frequency close to the natural frequency gets slightly displaced at a lower height and get wider. For higher frequencies, a much thinner wake is visible. As the shedding is suppressed up to further downstream positions, the upper and lower shear layers do not spread as much.

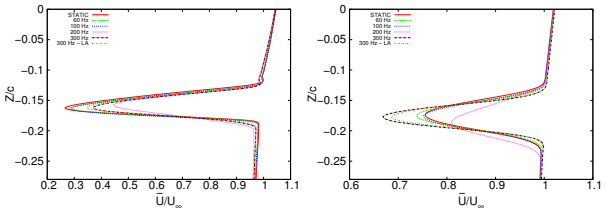

(a) $x/c = 1.1$ (b) $x/c = 1.4$

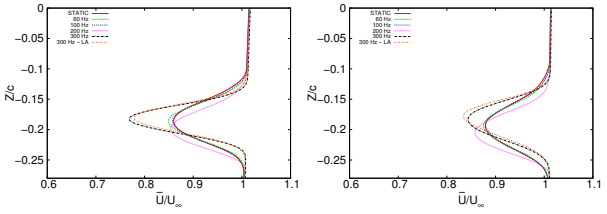

(c) $x/c = 1.7$ (d) $x/c = 2.0$

Figure 9: Comparison of mean longitudinal velocity profiles along the wake for various actuating frequencies. The amplitude is set at $0.35mm$ for every morphing application, except for the 300Hz-LA (lower amplitude) case where a value of $0.15mm$ was used.

Fig. 10 attests to this effect. The values for the wake width and for the spreading rate of both shear layers are presented. The spreading rate here is defined with the distance for which the halving of the velocity is achieved ($z^*_{50\%}$). In Fig. 10a the thinning of the wake is presented due to the suppression of the shedding. Increasing the frequency to even higher values (i.e. $370Hz$) seems to weaken this shedding delay. Fig. 10b exhibits the decrease of the spreading of the upper shear layer which gets overpowered by the strengthened lower one, the interactions become weaker and finally the resulting shedding mechanism is delayed as it has been previously shown.

- EFFECTS ON THE AERODYNAMIC FORCES

The effect on the aerodynamic forces is evaluated in this section. The lift and drag coefficients are compared in Fig. 11. In Fig. 11a and 11b the effect of the actuation frequency is presented for a constant amplitude of $0.35mm$ while in Fig. 11c and 11d the effect of the amplitude is examined.

Actuating in the region around the natural shedding frequency presents a prominent increase in both lift and drag mean values, accompanied however with a significant increase in the fluctuations (as indicated by the root

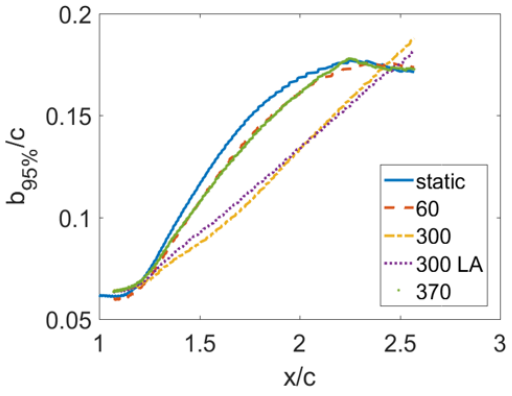

(a)

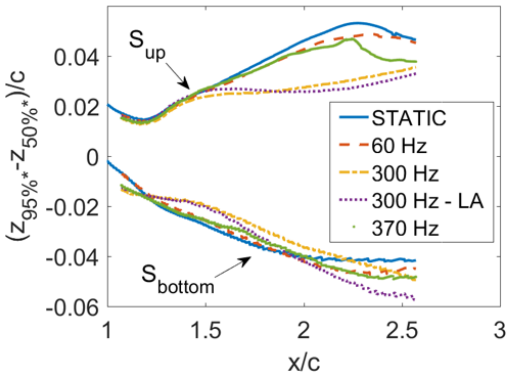

(b)

Figure 10: Comparison of the wake characteristics for various actuating frequencies. (a) Width of the wake with $b_{95\%} = z^{up}_{95\%} - z^{low}_{95\%}$, $z^*_{95\%}$ the position for which $u = 0.95 \cdot U_{inlet}$ and (b) Spreading rate of upper (S_{up}) and lower (S_{bottom}) shear layer. The amplitude is set at $0.35mm$ for every morphing application besides the 300Hz-LA (lower amplitude) case where a value of $0.15mm$ was used.

mean squared - rms - values) of the coefficients as well. This attests to the resonance observed in the previous section and is also in agreement with the experimental studies included in [4]. Acting with frequencies outside this region still provides an increase in lift and in some cases a decrease in drag, but always keeps the rms levels in lower values. In all the morphing cases the lift versus drag ratio increases, an effect that could not achieved with a static deformation of the trailing edge at the maximum displacements.

The amplitude variation indicates a linear response concerning the rms values which increase with the amplitude. The lift coefficient always increases while the drag coefficient initially decreases and then starts to increase. After a specific amplitude, the value of the drag is practically constant for the amplitudes examined in this article. Whether this plateau is higher or lower than the initial drag value without morphing depends on the frequency of the actuation.

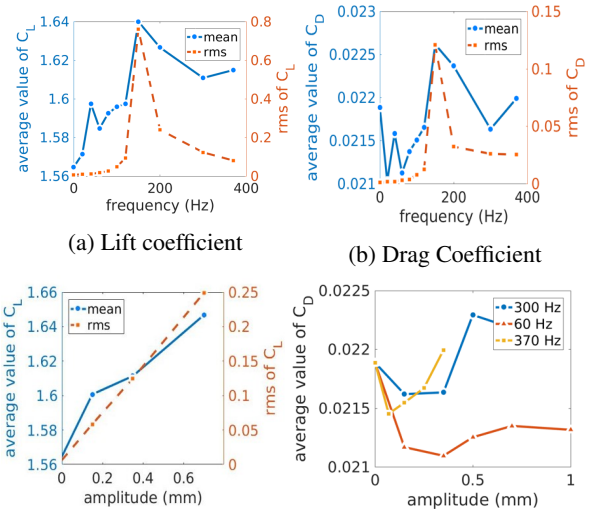

(a) Lift coefficient

(b) Drag Coefficient

(c) Lift coefficient

(d) Drag Coefficient

Figure 11: Effect on the aerodynamic coefficients versus frequency (top) variations with a constant amplitude of $0.35mm$ and versus amplitude (bottom) for a constant frequency of $300Hz$ (left) and various frequencies (right). Zero values for amplitude/frequency imply absence of morphing.

5.2 Proper Orthogonal Decomposition

The Proper Orthogonal Decomposition (POD) is applied here for the eduction and study of the coherent structures developed in the flow. The POD method was introduced first by Karhunen and Loweve and applied in Fluid Mechanics by Berkooz et al. [1]. The flow field solution is split in spatial modes and temporal coefficients sorted by their importance (relative energy) in the flow.

The Snapshot POD is applied here on the computational results for the two components of the velocity field. In this way there is a direct correspondence between the eigenvalues provided by the method and the kinetic energy of the flow. Two cases are examined here: the static one where no morphing is applied and the actuation at $300Hz$ where we have the most prominent effects in the wake development. In both cases the sampling time step was taken constant ($10^{-4}sec$) and a constant number of snapshots (619) were used to construct the POD data matrix.

In Fig. 12a the mode eigenvalues are plotted for the two cases. The first mode corresponding in the mean flow, exhibits the highest values as it represents the biggest portion of the flow's kinetic energy. Taking into account the modes corresponding to the fluctuating part of the flow (Fig. 12b) it can be deduced that less than 60 modes cover 98% of the fluctuating energy. The energy levels of the

first few fluctuating modes are increased in the morphing case and the slope of the cumulative fluctuating energy is reduced. While the energy of the first (mean) modes is in the same level (less than 1% difference) between the two cases, the total fluctuating energy is significantly increased in the morphing case.

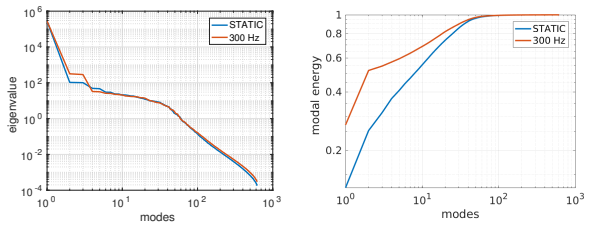

(a) Sorting of eigenvalues. (b) Relative fluctuating energy.

Figure 12: Eigenvalues of the modes sorted by the method (left) and relative cumulative energy (right) corresponding to the fluctuating part of the flow.

The spatial image of the modes as well as their temporal behaviour is significantly different between the two cases. For the case where no morphing is applied (Fig. 13), the modes 2 (coupled with mode 3) and 4 (coupled with mode 5) correspond to the shedding and initial instability respectively, observed also in the spectra. Mode 6 presents modulations of the shedding due to nonlinear interactions. Higher modes (not presented here) correlate with modulations and low frequency feedback effects. Mode 27 indicates the shear layer instability pattern. A frequency close to $350Hz$ is also identified in the same region and could be related to a separation bubble created on the pressure side, close to the trailing edge, due to the (supercritical) shape of the A320 wing. Modes of even higher order (above 50) are related to smaller scale fluctuations over the wake.

Considering the morphing case (Fig. 14) the following modifications are present. Mode 2 (coupled with mode 3) corresponds to the reinforcing of the shear layer close to the trailing edge. The temporal coefficient presents a development locked at the actuating frequency ($300Hz$) while the spectrum of mode 4 (coupled with mode 5) related to the secondary instability takes place at a frequency with half of this value. In this case, the von Kármán shedding seems to be contained only further downstream and to a less wide region as the wake becomes thinner as well. Modulations of the instabilities occur, indicating a move to different frequency ranges (mode 6) while harmonics of the actuation frequency appear as well causing further interactions. In mode 41, a structure resembling the one of mode 27 of the non-morphed case appears. As the energy of the fluctuations increases, previous modes are shifted in regions of relatively lower order. The predominant higher frequency at $350Hz$ appearing previously has vanished.

6. CONCLUSION

In this study the electroactive morphing effect created by mini-piezo-actuators disposed along the span of an Airbus-A320 wing has been studied by means of TRPIV and High-Fidelity numerical simulations. These actuators introduce optimal vibrations and slight deformations of the trailing-edge region. Having in disposal a detailed experimental database and newly acquired computational results, a combined examination of high Reynolds dynamics in the wake of this supercritical wing has been carried out in respect of aerodynamic performance increase. The main flow characteristics have been underlined. Various frequencies and amplitude combinations have been studied numerically to evaluate the morphing effects in order to enable future experiments around the same prototype, focusing on the most *optimal* morphing actuations.

The wake dynamics are significantly affected by the application of morphing when acting in frequencies close or above the natural frequencies of the separated shear layers. This has been emphasized by the POD analysis that has showed new modes emerging and taking the place of naturally existing modes in positions of higher relative energy. The aerodynamic performance gets enhanced as the mean value of the lift versus drag is found to be increased in every morphing case examined. By the present electroactive morphing concept, an order of 3.2% increase in lift has been achieved and at the same time a 1% decrease in the drag. Some frequencies studied provided even higher values of drag reduce. This enhancement of the aerodynamic performance was completely associated with the vibratory behaviour as slight static deformations of the trailing edge by the same amplitude did not produce analogous results.

ACKNOWLEDGEMENTS

The authors are grateful to the Engineering and Technical services of IMFT and LAPLACE Laboratories, to the Signal and Image Services of IMFT enabling the TR-PIV measurements, to the Software Services of IMFT enabling the MPI treatment of the TRPIV data bases on the supercomputer CALMIP, as well as to the three national supercomputing centers: CINES, IDRIS, CALMIP for having provided a significant CPU allocation for the present study. EU project www.smartwing.org/SMS/EU

REFERENCES

[1] G Berkooz, P. Holmes, and and J. L. Lumley. The Proper Orthogonal Decomposition in the Analysis of Turbulent Flows. *Annual Review of Fluid Mechanics*, 25(1):539–575, 1993.

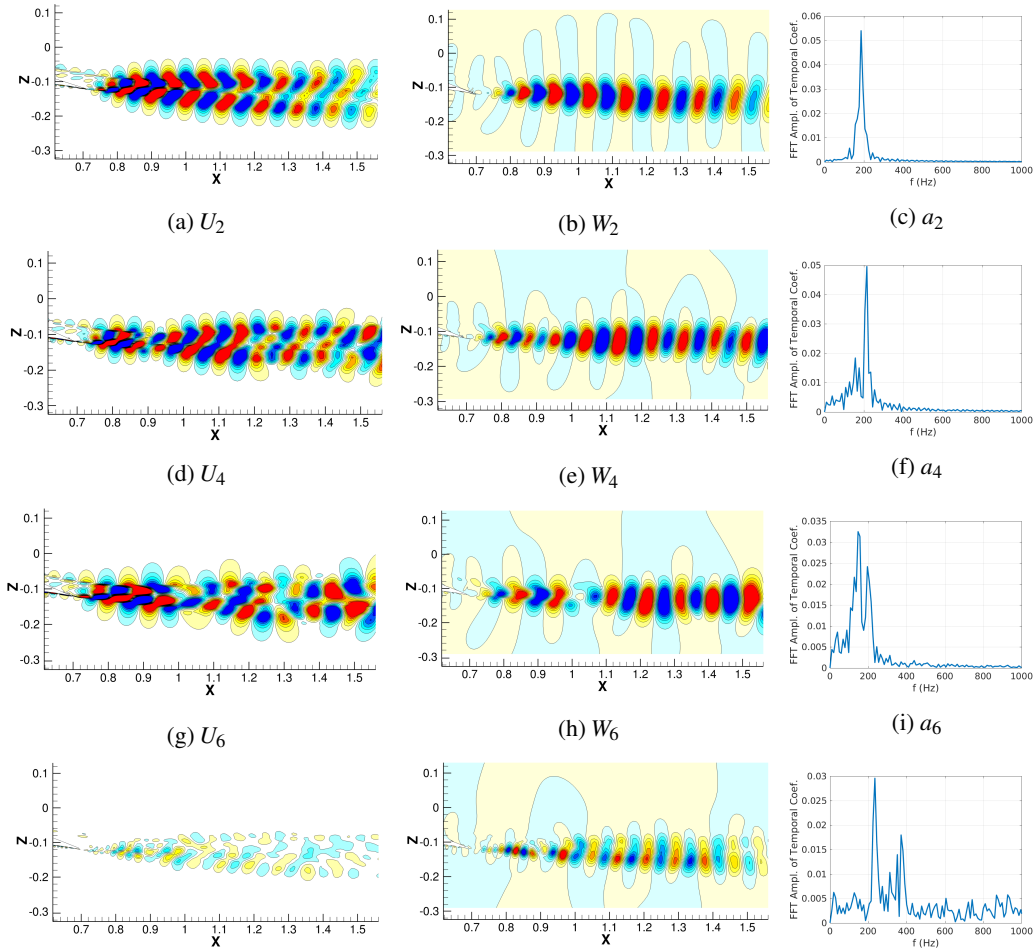

(a) U_2 (b) W_2 (c) a_2

(d) U_4 (e) W_4 (f) a_4

(g) U_6 (h) W_6 (i) a_6

(j) U_{27} (k) W_{27} (l) a_{27}

Figure 13: Spatial modes computed with the POD corresponding to the two velocity components and FFT of the respective temporal coefficients. Indices provide the order of the mode. The first (mean) mode is omitted. Case without morphing.

[2] R. Bourguet, M. Braza, G. Harran, and R. El Akoury. Anisotropic Organised Eddy Simulation for the prediction of non-equilibrium turbulent flows around bodies. *Journal of Fluids and Structures*, 24(8):1240–1251, November 2008.

[3] J. Donea, S. Giuliani, and J. P. Halleux. An arbitrary lagrangian-eulerian finite element method for transient dynamic fluid-structure interactions. *Computer Methods in Applied Mechanics and Engineering*, 33(1):689–723, September 1982.

[4] M. Gharib and K. Williams-Stuber. Experiments on the forced wake of an airfoil. *Journal of Fluid Mechanics*, 208:225–255, November 1989.

[5] C. Hirsch. *Numerical Computation of Internal and External Flows: The Fundamentals of Computational Fluid Dynamics*. Butterworth-Heinemann, Amsterdam, 2 edition, June 2007.

[6] Y. Hoarau, D. Pena, J. B. Vos, D. Charbonier, A. Gehri, M. Braza, T. Deloze, and E. Laurendeau. Recent Developments of the Navier Stokes Multi Block (NSMB) CFD solver. In *54th AIAA Aerospace Sciences Meeting*. American Institute of Aeronautics and Astronautics. DOI: 10.2514/6.2016-2056.

[7] R. F. Huang and C. L. Lin. Vortex shedding and shear-layer instability of wing at low-Reynolds numbers. *AIAA Journal*, 33(8):1398–1403, 1995.

[8] G. Jodin, V. Motta, J. Scheller, E. Duhayon, C. Dll, J. F. Rouchon, and M. Braza. Dynamics of a hybrid morphing wing with active open loop vibrating trailing edge by time-resolved PIV and force measures. *Journal of Fluids and Structures*, 74:263–290, October 2017.

[9] G. Jodin, J. Scheller, K. Jo. Rizzo, E. Duhayon, J.F. Rouchon, and M. Braza. Dimensionnement d'une

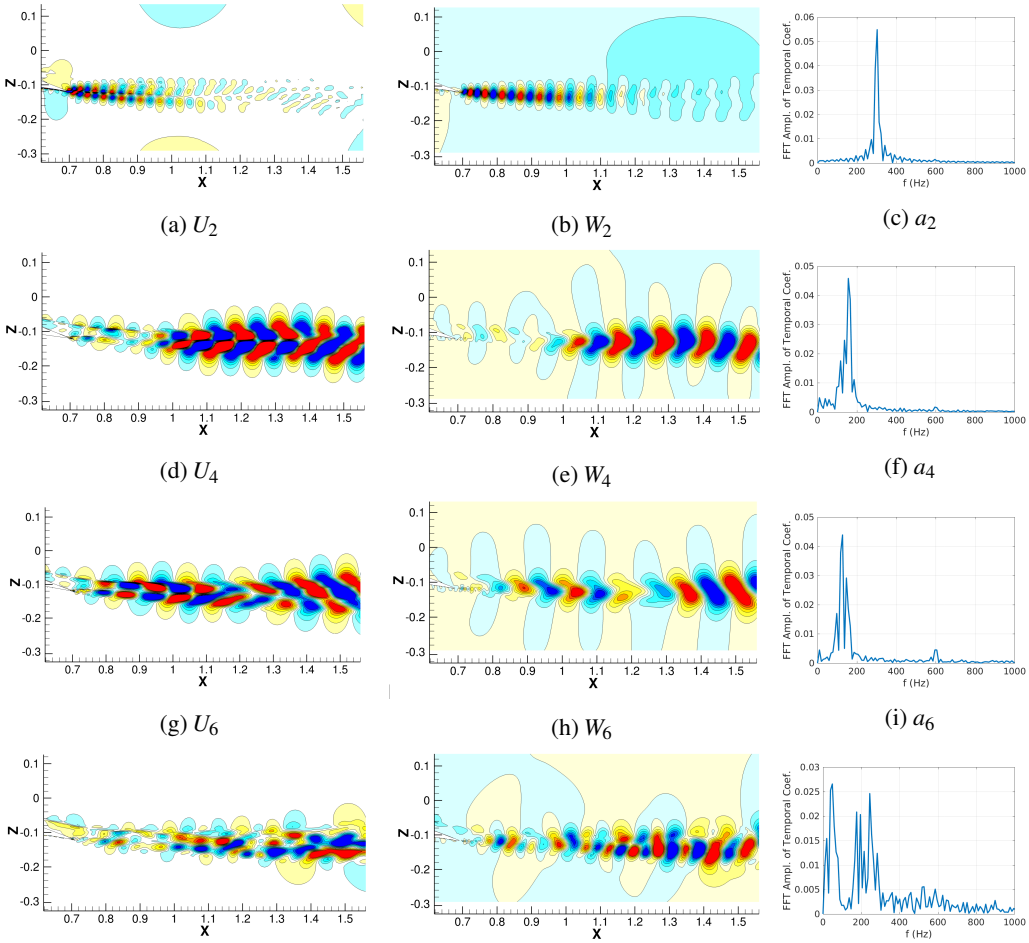

(a) U_2 (b) W_2 (c) a_2

(d) U_4 (e) W_4 (f) a_4

(g) U_6 (h) W_6 (i) a_6

(j) U_{41} (k) W_{41} (l) a_{41}

Figure 14: Spatial modes computed with the POD corresponding to the two velocity components and FFT of the respective temporal coefficients. Indices provide the order of the mode. The first (mean) mode is omitted. Morphing case at $300Hz$.

maquette pour l'investigation du morphing lectroactif hybride en soufflerie subsonique. pages pp. 1–13, 2015.

[10] A. Roshko. Experiments on the flow past a circular cylinder at very high Reynolds number. *Journal of Fluid Mechanics*, 10(3):345–356, May 1961.

[11] J. Scheller, M. Chinaud, JF. Rouchon, E. Duhayon, S. Cazin, M. Marchal, and M. Braza. Trailing-edge dynamics of a morphing NACA0012 aileron at high Reynolds number by high-speed PIV. *Journal of Fluids and Structures*, 55(Supplement C):42–51, May 2015.

[12] J. Scheller, M. Chinaud, JF. Rouchon, E. Duhayon, S. Cazin, M. Marchal, and M. Braza. Trailing-edge dynamics of a morphing NACA0012 aileron at high Reynolds number by high-speed PIV. *Journal of Fluids and Structures*, 55:42–51, May 2015.

[13] J. Scheller, G. Jodin, K. J. Rizzo, E. Duhayon, J.F. Rouchon, M. S. Triantafyllou, and M. Braza. A combined smart-materials approach for next-generation airfoils. *Solid State Phenomena*, vol. 251(DOI:10.4028/www.scientific.net/SSP.251.106):pp. 106–112, 2016.

[14] D. Szubert, F. Grossi, A. Jimenez Garcia, Y. Hoarau, J. C. R. Hunt, and M. Braza. Shock-vortex shear-layer interaction in the transonic flow around a supercritical airfoil at high Reynolds number in buffet conditions. *Journal of Fluids and Structures*, 55:276–302, May 2015.

[15] S. Yarusevych, P. E. Sullivan, and J. G. Kawall. On vortex shedding from an airfoil in low-Reynolds-number flows. *Journal of Fluid Mechanics*, 632:245–271, August 2009.

N. Simiriotis, G. Jodin, A. Marouf, Y. Hoarau, J.F. Rouchon, M. Braza, Award 3AF « Association d'Aerinautique et Astronautique - France » of best article presented at the 53th AERO2018 Conference, Salon de Provence, March 2018, Journal of 3AF N° 39, 2019, Page 18, https://www.3af.fr/sites/default/files/lettre-3af-39-110919-preview-2.pdf?utm_source=LETTRE+3AF+37&utm_campaign=b427fcbe47-3AF_Lettre_28_COPY_01&utm_medium=email&utm_term=0_9069af461d-b427fcbe47-180245357

NUMÉRO 39
SEPTEMBRE - OCTOBRE 2019

3AF
Association Aéronautique et Astronautique de France

LETTRE 3AF
La revue de la société savante de l'Aéronautique et de l'Espace

communication sous forme d'article dans l'*International Journal of Numerical Methods for Heat & Fluid Flow (IJNMHFF)* qui va consacrer un numéro spécial à la publication d'une sélection des meilleures communications, après la procédure d'évaluation habituelle par des experts, initiative qui permettra de valoriser ces travaux.

AUTRES MANIFESTATIONS

Le banquet traditionnel dans le très beau cadre de la brasserie Bofinger a été l'occasion de remettre le prix 3AF de la meilleure communication présentée à la dernière conférence (AERO2018 à l'École de l'air de Salon-de-Provence sur le thème *Multiphysics approach in Aerodynamics).*

Les lauréats étaient Nicolaos Simiriotis, Gurvan Jodin, Abderahmane Marouf, Yannick Hoarau, Jean-François Rouchon et Marianna Braza de l'IFMT, Institut ICUBE et Laboratoire Laplace. La journée du mardi 26 s'est terminée par une visite guidée du magnifique Musée des Arts et Métiers.

Remise du prix de la meilleure communication à AERO2018 à Salon-de-Provence